ORGEL, L. E. (1958). *J. Chem. Soc.* pp. 4186–4190.
OUVRARD, G. & BREC, R. (1990). *Eur. J. Solid State Inorg. Chem.* **27**, 477–488.
OUVRARD, G., BREC, R. & ROUXEL, J. (1985). *Mat. Res. Bull.* **20**, 1181–1189.
OUVRARD, G., FRÉOUR, R., BREC, R. & ROUXEL, J. (1985). *Mat. Res. Bull.* **20**, 1053–1062.
PETŘÍČEK, V. (1995). *SDS95*. Institute of Physics, Praha, Czech Republic.
PROUZET, E., OUVRARD, G. & BREC, R. (1986). *Mat. Res. Bull.* **21**, 195–200.
WIEDENMANN, A., ROSSAT-MIGNOD, J., LOUISY, A., BREC, R. & ROUXEL, J. (1981). *Solid State Commun.* **40**, 1067–1072.
ZHUKOV, V., BOUCHER, F., ALEMANY, P., EVAIN, M. & ALVAREZ, S. (1995). *Inorg. Chem.* In the press.

*Acta Cryst.* (1995). B**51**, 961–972

# X-ray and Neutron Diffuse Scattering in $LiNbO_3$ from 38 to 1200 K

BY N. ZOTOV,† F. FREY, H. BOYSEN, H. LEHNERT, A. HORNSTEINER AND B. STRAUSS

*Institut für Kristallographie und Mineralogie, Universität München, Theresienstrasse* 41, 80333 *München, Germany*

R. SONNTAG, H. M. MAYER AND F. GÜTHOFF

*Hahn–Meitner Institut, BENSC, Glienickerstrasse* 100, 14109 *Berlin, Germany*

AND D. HOHLWEIN

*Institut für Kristallographie, Universität Tübingen c/o Hahn–Meitner Institut, Glienickerstrasse* 100, 14109 *Berlin, Germany*

(*Received* 4 *November* 1994; *accepted* 23 *March* 1995)

## Abstract

A semi-quantitative description of X-ray and neutron diffuse scattering from *congruent* lithium niobate, $LiNbO_3$, is given. The diffuse scattering is concentrated in three sets of diffuse planes perpendicular to the pseudo-cubic symmetry-related [221], [241] and [$\bar{4}$21] directions and can be attributed to one-dimensional displacive and chemical disorder along these directions. The variation of the X-ray and neutron diffuse intensities with the scattering vector, as well as the comparison between X-ray and neutron data, indicate that more than one type of atom is involved. Temperature variations are followed from 38 to 1200 K. Different disorder models are discussed. The increase of the integrated intensities of the diffuse lines along the $[0\,1k\,2l]^*$ and $[0\,\bar{1}k\,4l]^*$ directions (*i.e.* sections of the diffuse planes) up to 800 K followed by a slight decrease at higher temperatures may be interpreted either by static disorder related to temperature-dependent variation of disorder/defect clusters or by dynamic disorder. Inelastic neutron scattering experiments do not show any anomaly of the transversal acoustic (TA) modes.

## 1. Introduction

After the discovery of the ferroelectric properties of lithium niobate ($LiNbO_3$), its average structure has been extensively studied (Abrahams, Reddy & Bernstein, 1966; Abrahams, Hamilton & Reddy, 1966; Abrahams & Marsh, 1986; Iyi *et al.*, 1992; Boysen & Altorfer, 1994; Zotov, Boysen, Frey, Metzger & Born, 1994). Lithium niobate (denoted LN hereafter) melts incongruently. Its structure and physical properties depend strongly on the Li:Nb ratio (Räuber, 1978) and can be substantially changed by small amounts of dopant ions. It is therefore important to understand the defects and the corresponding defect structures. Different models have been discussed in the literature (Lerner, Legras & Dumas, 1968; Nassau & Lines, 1970; Bollmann & Gernand, 1972; Peterson & Carnevale, 1972; Donnerberg, Tomlinson, Catlow & Schirmer, 1989; Schirmer, Thiemann & Wöhlecke, 1991; Metzger, 1993). All these models represent short-range order arrangements of a small number of vacancies around the $Nb_{Li}$ (Nb on Li sites) atoms, including ilmenite-type defects. However, none have been confirmed experimentally.

Direct information about the real structure can be obtained by measurement of the diffuse scattering. X-ray diffuse scattering from LN and $LiTaO_3$ was first reported

† On leave from the Institute of Applied Mineralogy, Rakovskistreet 92, Sofia 1000, Bulgaria.

by Zhdanov, Ivanov, Kolontsova & Korneev (1978) and Ivanov, Korneev, Kolontsova & Venevtsev (1978). They observed non-radial 'streaks', *i.e.* diffuse lines, passing through diffuse maxima. The diffuse lines were assigned to three sets of diffuse planes perpendicular to the directions of the Li—O—Li—... or Nb—O—Nb—... chains. The intensity ratio of the diffuse streaks to the diffuse maxima ($I_{\text{diff.streak}}/I_{\text{diff.max}}$) was reported to increase by a factor of five with increasing temperature between 293 and 1023 K. However, the diffuse maxima on their X-ray photographs (Fig. 1*b* in their paper) are heavily overexposed. Further high-temperature diffraction studies of LN have been performed mainly in connection with the character of the phase transition in LN (Abrahams, Levinstein & Reddy, 1966; Boysen & Altorfer, 1994).

The aim of the present paper is to investigate the defect structure of congruent lithium niobate ([Li]:[Nb] = 0.947) in more detail by means of X-ray and neutron diffuse scattering at different temperatures in order to determine the static *versus* dynamical origin of the diffuse scattering. For this purpose some preliminary inelastic neutron scattering experiments were also performed.

## 2. Experimental

The crystals used were commercially available (Crystal Technology, Palo Alto, USA) congruent lithium niobate ($Li_{0.947}Nb_{1.011}O_3$), single crystal wafers (0.5 mm thickness each).

The X-ray diffraction patterns at room temperature were taken by both the Noromosic (non-rotating monochromatic single crystal) photographs [quartz (10.1) monochromator, Mo $K\alpha$ radiation, exposure times typically 40–60 h] and the precession method (Mo $K\alpha$, exposure time 500 h, rotating anode). The relative intensities on the X-ray photographs were determined with a HP ScanJet IIc Scanner using the procedure described by Proffen & Hradil (1993). Low-temperature photographs were taken at 70 and 120 K using a low-temperature Weissenberg camera (quartz monochromator, Mo $K\alpha$ radiation, 140 h exposure time; Adlhart & Huber, 1982). The high-temperature X-ray diffraction experiments were performed using both a high-temperature Weissenberg camera (Adlhart, Tzafaras, Sueno, Jagodzinski & Huber, 1982) and an Enraf–Nonius CAD-4 single crystal diffractometer (graphite monochromator, Mo $K\alpha$ radiation) equipped with a mirror furnace. The quality of the sample crystals after cooling or heating was checked by additional X-ray photographs taken at room temperature.

The neutron diffuse scattering experiments were performed at BENSC-HMI, Berlin, on the flat-cone diffractometer E2 (Hohlwein, Hoser & Prandl, 1986) equipped with a curved multidetector covering a $2\theta$ range of 80° using $\lambda = 1.217$ Å and 30′ collimation before the monochromator. Low temperatures down to 38 K were achieved with a standard He cryostat. Measurements in the (0*kl*) plane were carried out by rotating the crystal with step width $\Delta\omega = 2°$ using first a stack (20 × 20 × 30 mm) of oriented single crystal wafers. Due to the non-negligible absorption (Li!), we reduced the size of the sample to 8 × 8 × 20 mm afterwards and used a smaller step width of 0.2°.

The inelastic neutron scattering experiments were performed on the triple-axis spectrometer E7 at BENSC-HMI/Berlin. The measurements were performed in constant $k_i$ mode [pyrolitic graphite (PG) filter in the incident beam, PG(002) monochromator and analyser, $\lambda = 2.38$ Å, collimations 60′–40′–40′–60′] at room temperature and at about 750 K using a mirror furnace (Lorenz, Neder, Marxreiter, Frey & Schneider, 1993). The sample was in this case a stack of oriented single crystal wafers 6 × 20 × 20 mm in size.

## 3. Average structure

LN undergoes a ferro-paraelectric phase transition at *ca* $T_c = 1485$ K (Räuber, 1978). In the low-temperature ferroelectric phase LN has the space group $R3c$ with two formula units per primitive unit cell and lattice constants $a = 5.15$ and $c = 13.86$ Å. The high-temperature paraelectric phase has $R\bar{3}c$ space-group symmetry (Niizeki, Yamada & Toyoda, 1967) with a statistical distribution of the Li atoms on both sides of the oxygen planes (Boysen & Altorfer, 1994).

The structure of $LiNbO_3$ may be derived from a hexagonally closed-packed (h.c.p.) array of the O atoms in which 2/3 of the octahedral sites are occupied by the Nb and Li atoms. Nb and Li atoms lie on the threefold axis, while the O atoms are in general positions. The cation sequence along the threefold axis is ...Nb Li □ Nb Li □..., where □ denotes a vacancy. The distorted octahedra are linked together by common faces along the *c* axis, forming equidistant oxygen layers perpendicular to the *c* axis with distance *c*/6. Corner-linked $NbO_6$ and $LiO_6$ octahedra produce the chains mentioned in the *Introduction*. The relation of the actual structure to the h.c.p. and the perovskite structure has been discussed by Megaw (1968) and Megaw & Darlington (1975). The positions of the atoms are (hexagonal setting)

| Atom | *x* | *y* | *z* |
|---|---|---|---|
| Nb | 0 | 0 | *w* |
| Li | 0 | 0 | $1/3 + w'$ |
| O | *u* | $1/3 + v$ | 1/12 |

where the parameters $w, w', u$ and $v$ describe the deviations from the ideal h.c.p. structure. The parameter $u$ is related to the rotation $\omega$ of the octahedra around the triad axes [$\text{tg}\omega = 3.3^{1/2}u/(2 - 3u)$] and describes a continuous change from h.c.p. ($u = 0$, $\omega = 0°$) to perovskite ($u = 1/6$, $\omega = 30°$). The actual values of the distortion parameters depend on the [Li]:[Nb] ratio. While $w$, $w'$ and $v$ can be considered to be almost equal,

the values of $u$ decrease with decreasing off-stoichiometry (*cf.* Iyi *et al.*, 1992), *i.e.* there is a tendency for increasing $\omega$ with increasing off-stoichiometry. This indicates a coupling between the substitutional and displacive disorder in non-stoichiometric LN. It is interesting to note that this angle also increases with increasing temperature (Boysen & Altorfer, 1994), *i.e.* with increasing dynamical disorder. Hence, both static and dynamic disorder tend to change the LN structure towards the perovskite structure.

The presence of excess $Nb_2O_5$ in the crystal structure of non-stoichiometric LN requires the additional Nb atoms to be distributed among the Li and the empty octahedra. Several defect models of the *average* structure of LN have been proposed in the literature. Recent X-ray and neutron diffraction refinements (Iyi *et al.*, 1992; Zotov, Boysen, Frey, Metzger & Born, 1994) have confirmed the Li-vacancy model $[Li_{1-5x}Nb_x\square_{4x}][Nb]O_3$. In this model the excess $Nb^{5+}$ ions and the corresponding charge-compensating vacancies occupy only the regular Li sites. From combined X-ray and neutron powder refinements (Zotov, Boysen, Schneider & Frey, 1994), however, it cannot be completely excluded that a small amount of Nb (<0.1%) can also occupy the normally empty octahedral sites.

## 4. Results and discussion of room-temperature observations

### 4.1. *X-ray diffuse scattering*

Fig. 1 shows an oscillation photograph (±5°) taken at room temperature with the crystal oriented with the $a$ axis perpendicular to the primary beam and a corresponding calculated pattern (see below). The diffuse scattering is concentrated in three sets of diffuse lines crossing each other at the Bragg peaks. They are relatively sharp and extend over large portions of reciprocal space. A series of Noromosic photographs made by successive rotations of the crystal in steps of 5° around the $c$ axis (*cf.* Fig. 9) indicated clearly that the diffuse lines are in fact sections of parallel diffuse planes in reciprocal space. [In order to avoid confusion we use the term diffuse 'lines' instead of 'streaks', which is usually reserved for one-dimensional (1-D) diffuse phenomena in reciprocal space.]

The orientation of these diffuse planes has been determined from several Weissenberg photographs. In the ($hk0$) plane three sets of diffuse lines were observed – the first passing through reflexions satisfying the condition $2h + 4k = 6m$, the other two being weaker and passing through reflexions fulfilling the conditions $2h - 2k = 6n$ and $-4h - 2k = 6p$, respectively. In the ($0kl$) plane two sets of diffuse lines were observed: the first passing through reflexions with indices satisfying the condition $4k + l = 6m$, the second weaker and passing through reflexions satisfying the condition $-2h + l = 6n$. The directions in real space perpendicular to them are $[2\bar{2}1]$, [241] and $[\bar{4}\bar{2}1]$, respectively. This is probably not in contradiction with the assignment made by Zhdanov, Ivanov, Kolontsova & Korneev (1978), according to which the diffuse lines are perpendicular to the $[\bar{2}21]$ direction in real space, as they may have used a different setting.

The $[2\bar{2}1]$, [241] and $[\bar{4}\bar{2}1]$ directions are related by the threefold symmetry axis and are inclined at 52° to the $c$ axis (see Fig. 2). They coincide with the main axes of the so-called pseudo-cubic setting [(Räuber, 1978) *i.e.* the main axes of the related perovskite structure] and run parallel to the structural chains mentioned above. The reciprocal planes perpendicular to these directions obey

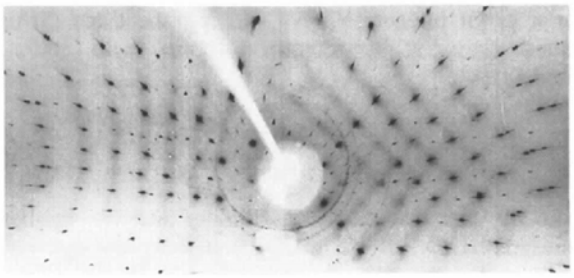

(*a*)

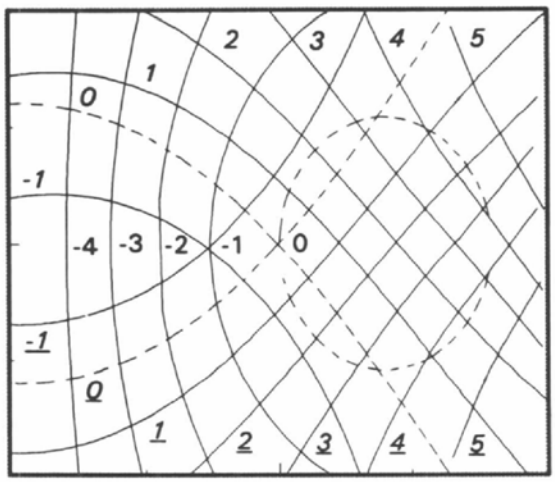


(*b*)

Fig. 1. (*a*) Oscillation photograph (±5°) with the incident beam perpendicular to the $a$ axis at room temperature (Mo $K\alpha$ radiation, 60 h exposure time). On the left-hand side the diffuse lines belong to a set of diffuse planes with the normal perpendicular to the $a$ axis (*i.e.* parallel to [241], *cf.* Fig. 2), on the right-hand side two sets parallel to $[\bar{4}\bar{2}1]$ and $[2\bar{2}1]$ are visible. (*b*) Calculated Noromosic pattern corresponding to (*a*). The numbering relates to the three sets of diffuse planes perpendicular to $[\bar{4}\bar{2}1]$ (italics), $[2\bar{2}1]$ (underlined italics) and [241] (roman). In each set the (absent) zero layer is indicated by a dashed line, the common crossing of these lines marks the origin.

Table 1. *Intersection of the diffuse planes with* (*a*) (*hk*0) *and* (*b*) (0*kl*) *planes*

| Direction | Intersecting line | Intersecting angle (°) |
|---|---|---|
| (*a*) | | |
| [2$\bar{2}$1] | (1$\bar{1}$0) | 52.15 |
| [241] | (2$\bar{1}$0) | 52.15 |
| [$\bar{4}\bar{2}$1] | ($\bar{1}$20) | 52.15 |
| (*b*) | | |
| [2$\bar{2}$1] | (012) | 48.60 |
| [241] | (0$\bar{1}$4) | 90.00 |
| [$\bar{4}\bar{2}$1] | (012) | −48.60 |

the following equations

$$\begin{aligned} 2h - 2k + l &= N_1 \\ 2h + 4k + l &= N_2 \\ -4h - 2k + l &= N_3. \end{aligned} \tag{1}$$

For a given integer, $N_1$, $N_2$ and $N_3$, the three diffuse planes cross at a reciprocal point with rational coordinates

$$\begin{aligned} h &= (N_1 - N_3)/6;\ k = (N_2 - N_1)/6; \\ l &= (N_1 + N_2 + N_3)/3. \end{aligned} \tag{2}$$

From the fact that on the oscillation and Weissenberg photographs the diffuse lines are passing through only Bragg reflexions, it can be concluded that $N_1$, $N_2$ and $N_3$ must be multiples of 6.

The directions of the intersecting lines of these diffuse planes with the (*hk*0) and (0*kl*) planes (for $N_1 = N_2 = N_3 = 0$), as well as the corresponding intersecting angles, are given in Table 1. The intersecting angle $\eta$ between the (*hk*0) and (0*kl*) planes with the diffuse planes is given by $\eta = \arccos[1/(1 + 12\xi^2)^{1/2}]$ and $\eta = \arccos[3/(1 + 1/\xi^2)^{1/2}]$, respectively, where $\xi = a/c$ (for congruent LN, $\xi = 0.3715$). The angle $\delta$ between the [2$\bar{2}$1], [241] and [$\bar{4}\bar{2}$1] directions also depends on the axial ratio $\xi$

$$\delta = \arccos[(1 - 6\xi^2)/(1 + 12\xi^2)]. \tag{3}$$

For congruent LN $\delta = 86.3°$, *i.e.* close to 90°.

On a precession photograph of the zero-layer perpendicular to the [241] direction (Fig. 3) two sets of very weak diffuse lines are observed, crossing each other at the expected angle 86 ± 1°. There is an additional diffuse line inclined by 45° to the line system which is not yet understood and will be not discussed further in the following. A Noromosic photograph with the primary beam perpendicular to the [241] direction (Fig. 4) exhibits, as expected, horizontal (H) diffuse lines (perpendicular to the [241] direction) and two sets of vertical (V) diffuse lines, lying on both sides of the azimuth line and corresponding to the other two sets of

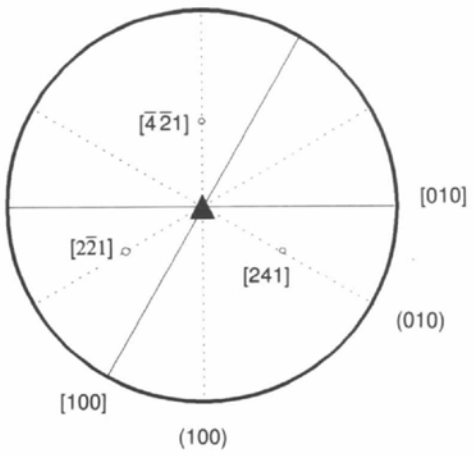


Fig. 2. Stereographic projection of the pseudo-cubic directions [241], [2$\bar{2}$1] and [$\bar{4}\bar{2}$1].

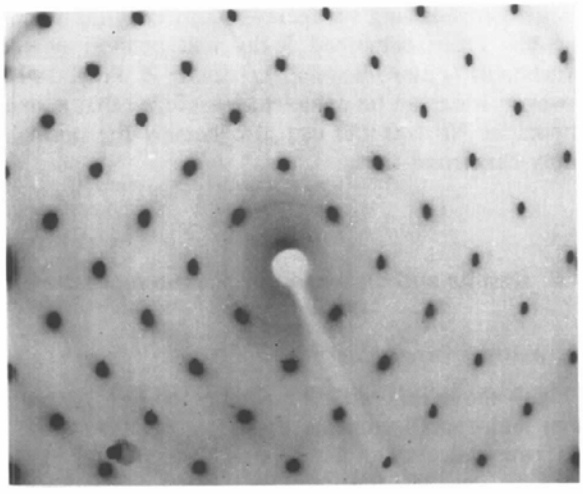

(*a*)

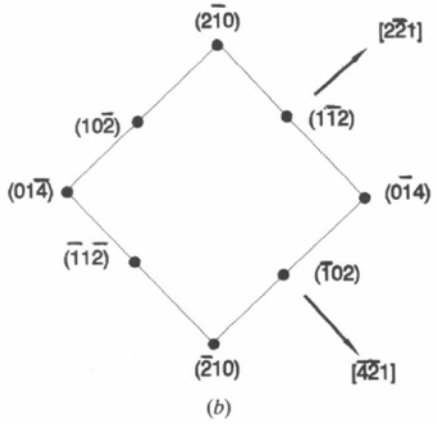


(*b*)

Fig. 3. (*a*) Zero-layer precession photograph perpendicular to the [241] direction; Mo $K\alpha$ radiation; 600 h exposure time (some asymmetry of the intensities left–right is due to slight misalignment). (*b*) Indices of the eight reflexions close to the origin and normals to the corresponding diffuse lines.

diffuse planes. In order to index the diffuse lines diffraction patterns were constructed by calculating the projections of the intersecting curves of the three sets of diffuse planes [described by (1)] and the Ewald sphere on a cylindrical film. These calculations show that the diffuse lines on the left side of Fig. 4 belong to diffuse planes perpendicular to the $[\bar{4}\bar{2}1]$ direction, while those on the right side to the $[2\bar{2}1]$ diffuse planes. An important observation is that there are no zero-layer diffuse lines. The fact that on Fig. 4 the H-lines are generally weaker than the V-lines can be attributed to the different orientation of the corresponding diffuse planes close to the Ewald sphere. While the [241] planes in this case cut the Ewald sphere perpendicularly, giving rise to the H-lines, those corresponding to the V-lines are inclined, thus matching the resolution function of the instrument to a larger extent.

As already pointed out, the diffuse planes cross each other in lines running exactly through Bragg peaks (see Figs. 1 and 3). That is why the intensity variations of the diffuse maxima at the crossing points of the H- and V-lines on Fig. 4 are mainly due to Bragg peaks accidentally touching the Ewald sphere, as well as due to thermal diffuse scattering (TDS) near the reciprocal lattice points. However, in addition, there is an underlying modulation of the diffuse planes with maxima coinciding with the Bragg peaks (*cf.* also Fig. 13).

Visual inspection of the intensity of the H-lines indicates that around the azimuth the $\pm 2$ diffuse lines are stronger than the $\pm 1$ and $\pm 3$ lines, while the situation is reversed at regions further away from the azimuth. This could indicate the presence of a helical structure element ($2_1$ axis).

A horizontal scan through the V-lines at $l = 1/2$ (Fig. 5) shows a variation of the intensity of the V-lines. In order to estimate quantitatively the variation of the FWHM and the integral intensities of the V-lines, similar scans on both sides of the zero line ($l \cong \pm 1/2$) were made on different X-ray Noromosic photographs. After subtracting the general background the diffuse maxima were fitted by Gaussians and the corresponding FWHM's and integral intensities from the different scans were averaged.

The integral intensity $I^n_{DS}$ of the $n$th diffuse line scanned across the diffuse plane is given by

$$I^n_{DS} = C|F^n_{DS}|^2 L_n P_n T_n A_n, \tag{4}$$

where $|F^n_{DS}|$ is the corresponding structure factor, $L_n$, $P_n$, $T_n$ and $A_n$ are the corresponding Lorentz, polarization, temperature and absorption factors, and $C$ is a scaling factor which depends on the intensity of the primary beam, exposure time, optical density of the X-ray film *etc.*

In order to exclude the constant $C$ we used normalized structure factors $R_{n,i}$

$$R_{n,i} = (I^n_{DS} L_i P_i T_i A_i)/(I^i_{DS} L_n P_n T_n A_n),$$

where $i$ numbers the selected normalizing diffuse line.

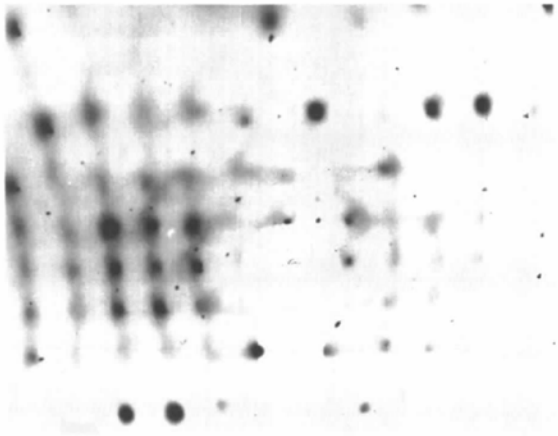

(*a*)

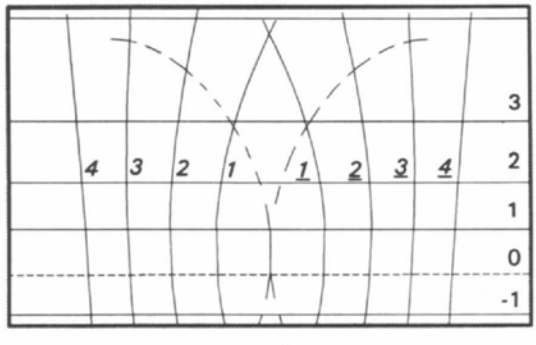


(*b*)

Fig. 4. (*a*) Noromosic photograph with the incident beam perpendicular to the [241] direction (Mo$K\alpha$ radiation, 60 h exposure time). (*b*) Calculated pattern (as in Fig. 1).

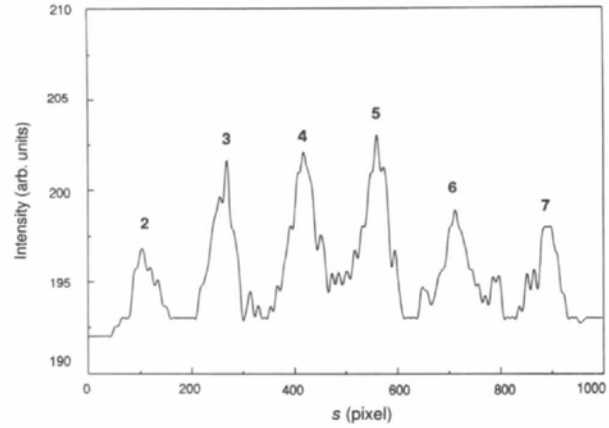


Fig. 5. Scan through the vertical diffuse lines on the left-hand side of Fig. 4 at $l = 1/2$ as recorded with a HP ScanJet IIc Scanner.

Further we assume that $T_n = \exp(-B_{DS}s_n^2)$, where $s_n = 2\sin(\theta_n)/\lambda$ is the scattering vector and $\theta_n$ the diffraction angle. $B_{DS}$ was taken as an overall isotropic temperature factor $B_{DS} = 1/3\ (B_{Li}^{eq} + B_{Nb}^{eq} + B_O^{eq}) = 0.65\,\text{Å}^2$, where $B_{Li}^{eq}$, $B_{Nb}^{eq}$ and $B_O^{eq}$ were taken from X-ray Rietveld refinements (Zotov, Boysen, Frey, Metzger & Born, 1994).

The Lorentz factors $L_n$ for integrated diffuse intensities obtained from scans perpendicular to diffuse planes are independent of $2\theta$ (Boysen & Adlhart, 1987), while the polarization factor $P_n$ for a primary beam monochromator has the standard form $P_n = (1 + \cos^2 2\theta_m \cos^2 2\theta_n)/(1 + \cos^2 2\theta_m)$, where $\theta_m$ is the diffraction angle of the monochromator.

In order to estimate the absorption correction we have approximated the $0.4 \times 0.4 \times 0.5$ mm crystal used for the Noromosic photographs as a cylinder with radius $R = 0.4$ mm. The transmission factors $A^* = 1/A$ for cylindrical samples with different $\mu R$ values were tabulated by Weber (1967) as a function of $2\theta$ from where the data for $\mu R = 2.1$ ($LiNbO_3$, Mo $K\alpha$ radiation) were taken. The actual values of $A_n^*$ were calculated by cubic spline interpolation.

While the FWHM's of the V-lines remain constant in first approximation within the error limits [average FWHM $= 0.075\,(5)\,\text{Å}^{-1}$], the normalized integral intensities $R_{n,2}$ increase non-linearly with increasing $s_n$ (Fig. 6). It is not clear whether the small maximum at *ca* $s = 1.2\,\text{Å}^{-1}$ reflects a real structural modulation or can be smoothed out within error limits.

### 4.2. *Neutron diffuse scattering*

From the above X-ray experiments alone it cannot be decided unambiguously which atom species are involved in the disorder. Therefore, for comparison, neutron diffraction experiments have been performed in order to take advantage of the substantial difference between the X-ray and the neutron scattering lengths [$b_{Nb} = 7.8$ fm, $b_O = 5.8$ fm and $b_{Li} = -2.0$ fm (Sears, 1992)].

A part of the diffuse scattering measured in the (0*kl*) plane is shown in Fig. 7(*a*). The radial diffuse streaks and the curved streaks parallel to $2\theta$ (along the multicounter) are instrumental effects of the E2 diffractometer and will not be discussed here. Two sets of diffuse lines should be observed in the (0*kl*) plane (*cf.* Table 1). However, we observe very weak diffuse intensity only parallel to the (012) direction superimposed by strong anisotropic TDS around the Bragg peaks (see below). The fact that we do not observe diffuse scattering along the (01$\bar{4}$) direction may be related to the fact that *two* sets of diffuse planes ([$\bar{4}$21] and [2$\bar{2}$1]), inclined by $\pm 48.6°$, intersect the scattering plane along the (012) lines, while only *one* set of planes ([241]) crosses perpendicularly to the (0*kl*) plane along the (01$\bar{4}$) lines.

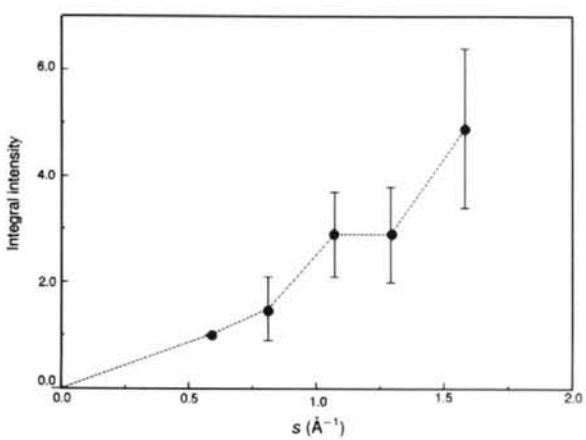


Fig. 6. Integral intensities of the vertical diffuse lines at $l = 1/2$ *versus* *s*. The intensities are corrected and normalized to the intensity of the second diffuse line.

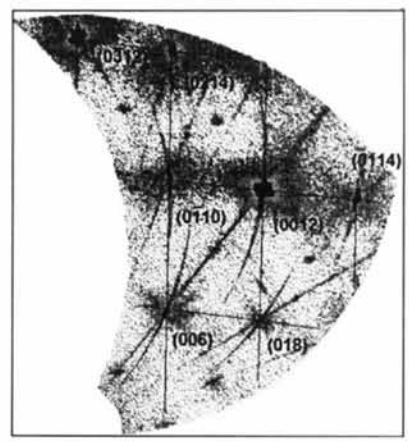


(*a*)

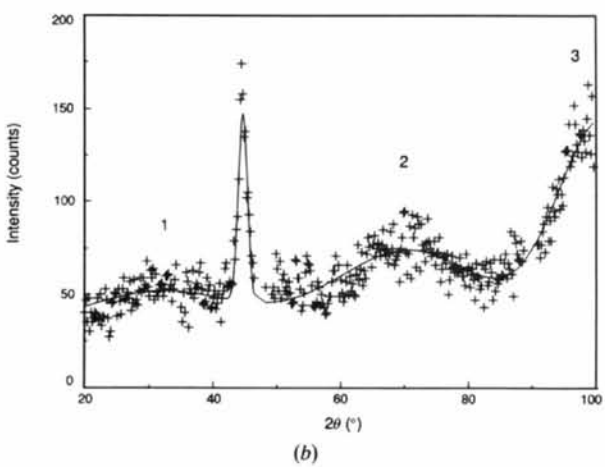


(*b*)

Fig. 7. (*a*) Neutron diffuse scattering in the (0*kl*) plane; The non-indexed diffraction peaks correspond to forbidden (0*kl*), $l = 2n + 1$ reflexions appearing due to 'Umweganregung' effects. (*b*) 1-D section through the (0*kl*) plane for a given setting of the crystal ($\omega = -6.1°$) and the 80° multicounter: (+) raw data points, solid curve: Gaussian fit.

Comparison of the intensity of the diffuse scattering in the (0*kl*) plane measured with *X-rays* (Weissenberg photographs) and *neutrons* shows that while in the first case the diffuse lines are strong along the (01$\bar{4}$) direction, in the neutron case they are strong along the (012) direction. This clearly indicates that the structure factor $|F_{DS}|$ contains more than one type of atom.

The variation of the intensity of the diffuse streaks measured with very high monitor rate for a $\omega = -6.1°$ setting of the crystal is given in Fig. 7(*b*). This orientation of the crystal corresponds to sections through the first three diffuse lines between (01.8) and (02.10), (00.12) and (01.14) and (01$\bar{1}$.16) and (00.18) reflexions, respectively. The sharp feature at *ca* $2\theta = 45°$ is due to the 'instrumental' radial streaking. As in the X-ray case, the intensity of the diffuse lines is very weak and increases with increasing *s*.

### 4.3. *Disorder models*

Since the diffuse scattering is restricted to planes in reciprocal space, the disorder is between ordered chains in real space parallel to the three pseudo-cubic directions [241], [2$\bar{2}$1] and [$\bar{4}\bar{2}$1] (called chain directions hereafter). In the structure of $LiNbO_3$ there are both —Li—Li— (—Li—O—Li—) and —Nb—Nb— (—Nb—O—Nb—) chains along these directions (Fig. 8). Apart from the extinction rule due to the pseudo-$2_1$-axis along the chains (see above), there is a general increase of the integral intensities of the diffuse lines with increasing *s* (Fig. 6). This behaviour would be consistent with purely displacive disorder. Since, however, the number of observed orders of planes is relatively small, some substitutionally disordered clusters (see below) cannot be excluded. From the absence of diffuse planes with $l = 0$ it may be concluded that the lateral packing of the disordered chains has an ordered projected structure, *i.e.* the displacements are exclusively along the chains. In case of substitutional disorder, we have to restrict the clusters to be one-dimensional (see below). The distance between the diffuse planes corresponds to the average translation period along the chains, which is the Li—Li (Nb—Nb) distance ($D = 3.8$ Å). From the additional independence of the FWHM's of the diffuse lines of *s* it can be concluded that a structural element of an *averaged* 1-D structure along a given chain preserves its translational character over large distances, thus excluding a 1-D liquid-like or 1-D random behaviour. This does not exclude the possibility of the occurrence of different 1-D clusters. The modulations on the diffuse planes indicate that there are lateral short-range correlations between the disorder elements in different chains.

As mentioned previously, more than one type of atom participates in the disordered chains. The substitutional defects are on the Li sites. Each $Nb_{Li}^{5+}$ ion requires four $\square_{Li}$ vacancies. Assuming local charge compensation it is quite natural to expect the $\square_{Li}$ vacancies in the immediate neighbourhood of the $Nb_{Li}$ defect, *i.e.* the formation of defect clusters along each of the chain directions such as Li—$Nb_{Li}$—□—Li, Li—□—$Nb_{Li}$—□, Li—□—□—$Nb_{Li}$ *etc.* with corresponding displacements of the neighbouring atoms. The size of such clusters (*ca* 11.4 Å) has been restricted to four cation sites in order to match the correlation length $L_c$ along the chains (*ca* 13 Å), calculated from the FWHM of the diffuse streaks. The quasi-extinction, mentioned above, indicates that most probably the clusters are not linear, but zigzag Li—O—$Nb_{Li}$—O—□—... chain segments. In the case of various types of defects, including *pairs of vacancies*, some randomness of the relative atomic displacements between the clusters (in different chains) may be expected.

An alternative purely displacive model can be isolated: $\square_{Li}$ and $Nb_{Li}$ defects randomly distributed on the lattice sites with the neighbouring Li atoms displaced towards (in the case of $\square_{Li}$) or away (in the case of $Nb_{Li}$) from the defect *along the chains*. The correlation length $L_c = 13$ Å can then be related to the number of atoms being displaced (note that the average separation between two defects along a given chain should be $2D \simeq 76$ Å). Again we expect diffuse maxima coinciding with the Bragg peaks.

Possibly the real disorder can be described by a combination of different disorder elements. Quantitative structure-factor calculations are necessary for a final decision.

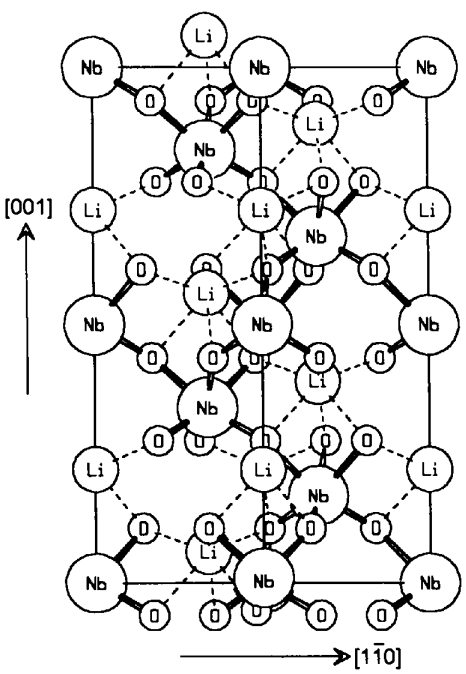


Fig. 8. Projection of the structure of lithium niobate perpendicular to the [110] direction.

## 5. Temperature dependence of diffuse scattering

### 5.1. *Low temperature*

Fig. 9 shows Noromosic X-ray photographs taken at 70 K and room temperature, with the $c$ axis perpendicular to the incident beam. At 70 K the intensity of the diffuse lines is mainly concentrated around the crossing points between the different sets. There is some asymmetry which is also present at higher temperatures. It may be concluded that at low temperatures the intensity of the homogeneous part of the diffuse scattering decreases substantially and the diffuse scattering is restricted mainly to the diffuse maxima located at the positions of the Bragg peaks.

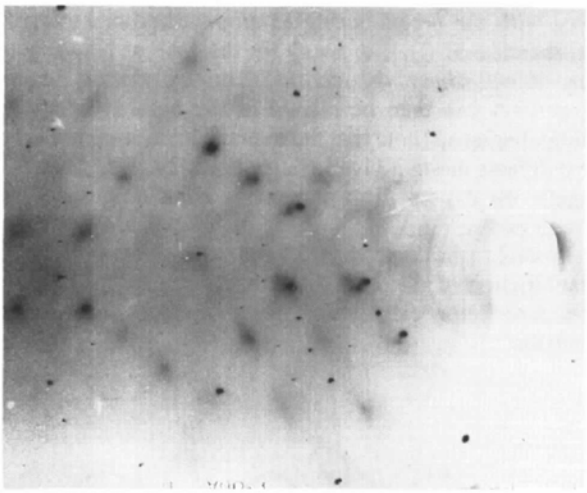

(*a*)

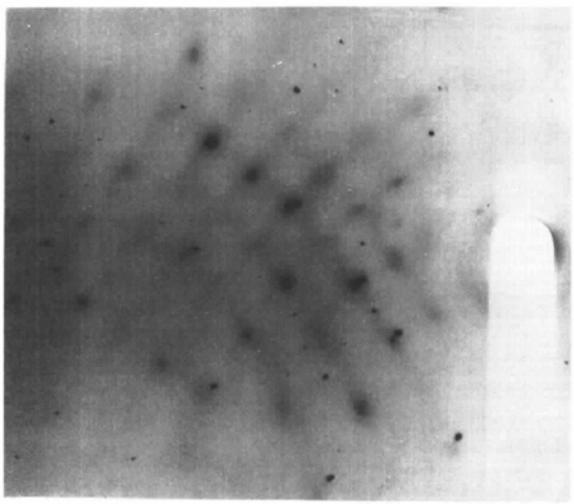

(*b*)

Fig. 9. Noromosic photograph with the incident beam perpendicular to the $c$ axis (Mo$K\alpha$ radiation, 140 h exposure time): (*a*) 70 K and (*b*) room temperature.

Therefore, at low temperatures the lateral correlations between the defect clusters discussed in §4.3 become quite substantial. With increasing temperature these correlations decrease, resulting in more random 1-D disorder. From the two photographs it cannot be decided unambiguously if these correlations do decrease gradually or if there is competition between correlated and uncorrelated disorder elements. More experiments are necessary to follow this process in detail.

Similar to the X-ray observations, at 38 K the neutron diffuse scattering is concentrated only close to the Bragg peaks (Fig. 10*a*). With increasing temperature both the diffuse scattering around the Bragg peaks and the intensity of the diffuse line along the $[0\,1k\,2l]^*$ direction, connecting the $(0\bar{2}.8)$, $(0\bar{1}.10)$ and (00.12) reflexions, increases (Fig. 10*b*).

The integrated intensities of the diffuse features close to the Bragg peaks increase with increasing temperature (Fig. 11), while the corresponding FWHM's remain

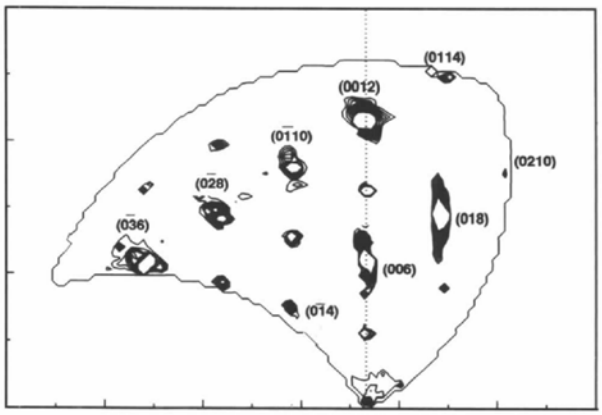


(*a*)

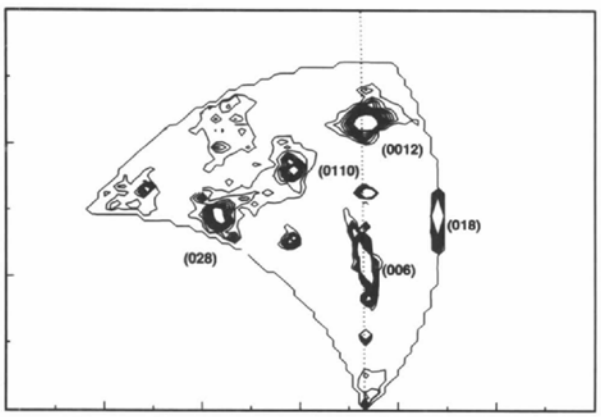


(*b*)

Fig. 10. Neutron diffuse scattering in the (0$kl$) plane: (*a*) 38 K and (*b*) room temperature. In both drawings the isolines start at 120 counts with increments of 50 counts. Instrumental artifacts (as in Fig. 7) excluded by fitting and smoothing procedure.

constant. Such behaviour can be interpreted by thermal diffuse scattering (TDS). In order to investigate this assumption, the shape of the TDS contours around several (0*kl*) reflexions has been calculated (Fig. 12) using the method of Wooster (1962) and the elastic constants of $LiNbO_3$ published by Smith & Welsh (1971). The direction of the elongation of the calculated TDS is, as experimentally observed, almost perpendicular to the scattering vector *s*. In general, it does not coincide with the direction of the diffuse streaks along the $[0\,1k\,2l]^*$ and $[0\,\bar{1}k\,4l]^*$ directions. This allows the separation of the TDS and the disorder diffuse scattering. The temperature dependence of the diffuse lines is discussed below, together with the high-temperature X-ray observations.

### 5.2. *High temperature*

X-ray Noromosic photographs such as Fig. 4 with the incident beam perpendicular to the [241] direction have been taken at 520, 770 and 970 K (the uncertainty of the measured temperatures is estimated to be between 50 and 100 K). In order to determine the temperature dependence of the integrated intensities, scans parallel to the layer lines at $l = 1/2$ have been made through the third and the fourth vertical streaks, which are the strongest at room temperature (see Fig. 5). The scanned traces were smoothed by Fourier filtering and fitted with Gaussian functions.

Additional high-temperature measurements were performed on an Enraf–Nonius CAD-4 single crystal diffractometer at 520 and 700 K. The exact temperatures in this case were determined from the temperature dependence of the lattice constants. Fig. 13 shows the diffuse scattering measured around the (054) reflexion with 100 s per point. It is concentrated close to the Bragg peak at room temperature and extends beyond the reciprocal lattice point (0 4.625 5.5), which is the zone boundary in the $[0\,\bar{1}k\,4l]^*$ direction. This figure confirms well the modulated structure of the diffuse planes. Note

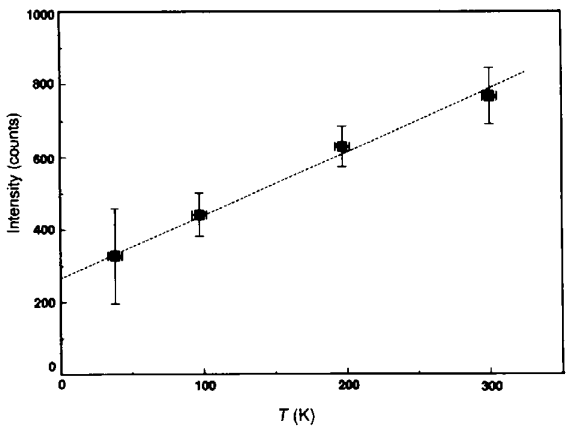


Fig. 11. Temperature dependence of the integral intensity of the TDS near the $(0\bar{1}.10)$ reflexion (neutron measurement).

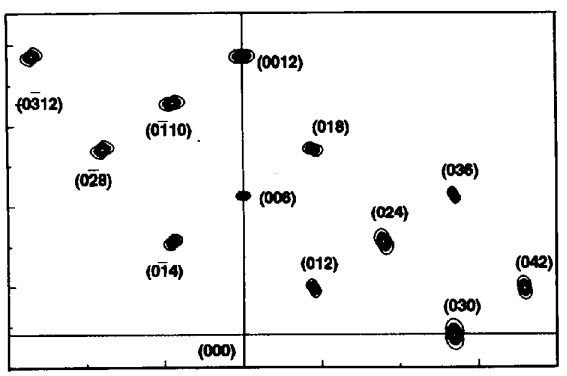


Fig. 12. Calculated TDS ellipsoids of some reflexions in the (0*kl*) plane.

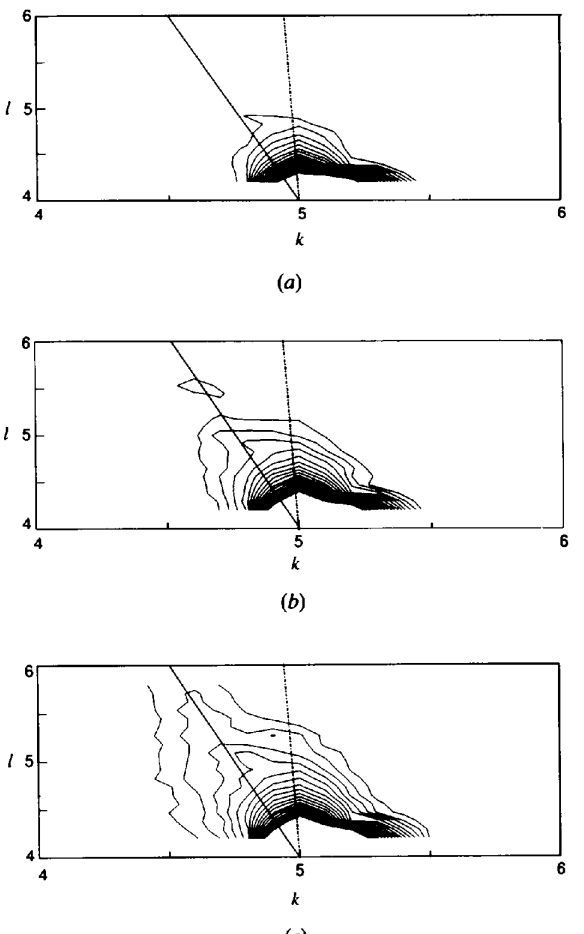


Fig. 13. Part of the diffuse scattering measured in the (0*kl*) plane with an Enraf–Nonius CAD-4 diffractometer (Mo$K\alpha$ radiation): (*a*) room temperature, (*b*) 523 and (*c*) 700 K. In all drawings the isolines start at 8000 counts with increments of 1000 counts. The solid line indicates the direction of the diffuse line, the dashed line the direction of the largest spread of the TDS.

that near this reflection the TDS can be clearly separated due to its different orientation (see also Fig. 12). In the other prominent direction $[0\,1k\,2l]^*$ there is practically no intensity, even at 700 K. In order to estimate quantitatively the temperature dependence of the diffuse scattering, one-dimensional scans at $l = 4.5$ have been made for each temperature and the resulting curves fitted with a Cauchy function.

In all three techniques the FWHM's of the diffuse lines remain more or less constant. The temperature dependence of the integrated intensities of the diffuse scattering is compared in Fig. 14. They are normalized to the corresponding integrated intensity measured at room temperature in order to exclude (approximately) the $s$-dependence. All data points up to 800 K lie very well on a straight line with the equation $I(T)/I(300\,\mathrm{K}) = 0.3\,(2) + 0.0021\,(7)T$. The non-zero intercept indicates that at least part of the diffuse scattering is of purely static origin. A non-zero intercept is also found for the TDS presented in Fig. 11, which probably indicates the same static component at this point. An influence of zero-point motion is very unlikely. Note also that in the case of a dynamic interpretation of the temperature-dependent parts, the intensity should follow the relation $I \propto s^2T\exp(-B'Ts^2)$, *i.e.* the normalization procedure described above is an approximation only. The single point at 970 K indicates, however, a subsequent decrease of the diffuse intensities (see Fig. 14), which is in contradiction with the observations of Zhdanov, Ivanov, Kolontsova & Korneev (1978). This decrease could be related to an inversion temperature characteristic for dynamic processes: $T_i = 1/2B's^2$ (see *e.g.* Willis & Pryor, 1975), where $B = B'T$ is the atomic displacement parameter. Using the room-temperature value $B = 0.65\,\text{Å}^2$, one obtains $T_i \approx 900$ K for the given value of $s$, which fits well with the observation.

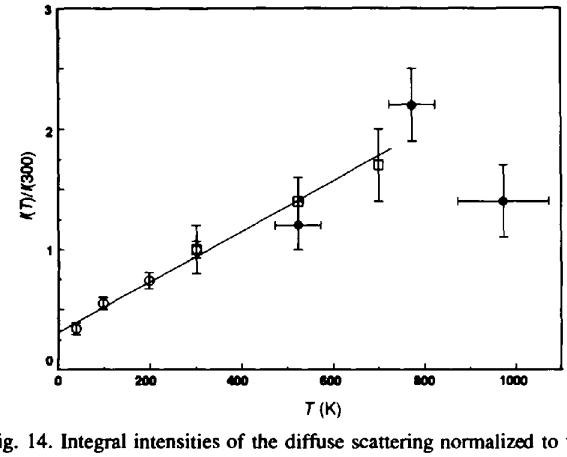


Fig. 14. Integral intensities of the diffuse scattering normalized to the intensity at room temperature $I(300\,\mathrm{K})$: ○ = low-temperature neutron measurement; □ = X-ray CAD-4 measurement; ● = X-ray high-temperature Noromosic photographs. The full line is a least-squares fit through the neutron and the CAD-4 data.

Apparently, the increase and subsequent decrease of the normalized intensities with increasing temperature can be interpreted in two ways. Either the intensity of the homogeneous part of the diffuse scattering first increases due to temperature-induced rearrangements of the defect clusters or displacement fields leading to a decrease of the lateral correlations between them, *i.e.* at the expense of the intensity of the diffuse maxima around the Bragg peaks. The subsequent decrease of diffuse intensity concentrated within the diffuse lines might reflect a change of the static disorder towards a more random behaviour of the defect clusters. This interpretation would be supported by the temperature-dependent variation of the non-stoichiometry of LN.

However, it can also be supposed that the increase of $I(T)/I(300\,\mathrm{K})$ is mainly due to a dynamic origin of the diffuse scattering (with an underlying static contribution). Note that the Li atoms become quite mobile at high temperatures (Boysen & Altorfer, 1994), *i.e.* there can be a rapid exchange with the empty sites. An argument in favour of the dynamical interpretaion is the fact that the TDS (Fig. 11) has a similar slope as the least-squares line in Fig. 14. It should be pointed out, however, that it is not normal TDS due to *long wavelength acoustic modes*, because this can be clearly separated in most cases, *i.e.* in this case we have to consider some low-lying dispersion surfaces similar to those found in perovskites such as $KNbO_3$. In principle, a definite decision can be made with the help of neutron inelastic scattering experiments.

## 6. Neutron inelastic measurements

The first neutron inelastic scattering measurements on LN were performed by Chowdhury, Peckham & Saunderson (1978) along the two main symmetry directions [001] and [010]. In order to investigate further a possible dynamical origin of the diffuse scattering in $LiNbO_3$, neutron inelastic scattering experiments at room temperature and *ca* 750 K have been performed. Unfortunately, with the given experimental set-up it was not possible to measure any phonons in the region of strong diffuse streaks. Nevertheless, in order to confirm the above assumption, namely that the extension of the diffuse streaks and the TDS can be separated at all temperatures, it is necessary to prove that there are no anomalies in the normal TA modes. Therefore, the acoustic dispersion branches along the (off-symmetry!) $[0\,\bar{1}k\,4l]^*$ and the $[0\,1k\,2l]^*$ directions have been measured around the (024) and (006) reflexions, respectively. Examples of constant $Q$ scans are shown in Fig. 15. The two dispersion branches measured are shown in Fig. 16. It can be seen that the initial slope of the dispersion branches coincides well with the sound velocities along the $[0\,\bar{1}k\,4l]^*$ and $[0\,1k\,2l]^*$ directions, calculated from the elastic constants. Comparison of the slopes of the measured TA phonons with those determined by Chowdhury, Peckham & Saunderson

(1978) along the [001] and [010] directions also indicates that there is no special anomaly in the phonon dispersion surface in the direction of the diffuse streaks. At higher temperatures the phonon intensities increase due to the $n(\omega)$ occupation factor. The slope of the dispersion curves decreases slightly, being more or less the same for the two investigated directions.

## 7. Concluding remarks

A detailed experimental study of the diffuse scattering in congruent lithium niobate ([Li]:[Nb] = 0.947) from low to high temperatures using both X-ray and neutron diffraction has been performed. The diffuse scattering is concentrated in three sets of diffuse planes perpendicular to the pseudo-cubic $[2\bar{2}1]$, [241] and $[\bar{4}\bar{2}1]$ directions in real space. Qualitatively the diffuse scattering can be related to 1-D displacive and substitutional disorder on the Li chains along these directions. Diffuse maxima around the Bragg positions reflect some 3-D short-range order of the defect elements. The homogeneous part of the diffuse planes reflects random distribution of the defect clusters. Unfortunately, it could not be decided unambiguously whether this contribution is of elastic origin and may then be related to the presence of different clusters, or if there is an underlying dynamical process of slowly fluctuating atomic positions. In the latter case the homogeneous part is of quasi-elastic origin.

At low temperatures *lateral* correlations between the defects result in confinement of the diffuse scattering into strongly asymmetric (X-ray case) diffuse maxima. With increasing temperature a change from 3-D short-range order to 3-D + 1-D chain disorder is observed. The intensity behaviour is not in conflict with a temperature-dependent static disorder, where the variation of the non-stoichiometry plays a decisive role. There are, however, also arguments in favour of dynamic disorder, in particular at high temperatures, with an underlying temperature-independent static component. Although not directly proven in the present experiment, the dynamic part could be related to a low-lying dispersion surface in agreement with the conclusions of Ivanov, Korneev, Kolontsova & Venevtsev (1978). The form and

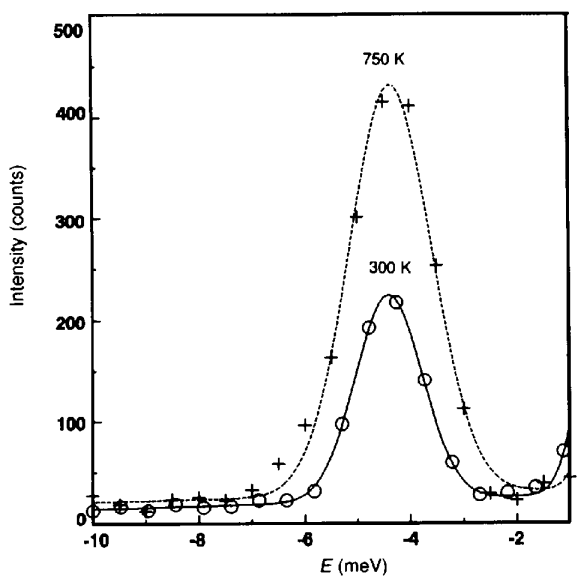


Fig. 15. Constant $Q$ scans at (0 1.925 4.3) measured at room temperature and 750 K.

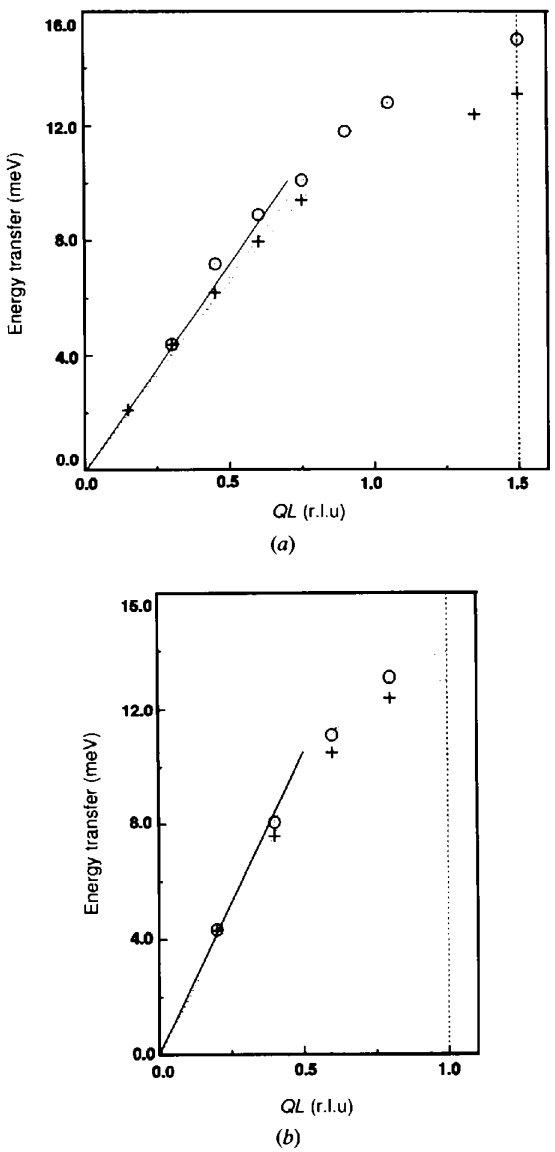


Fig. 16. The measured phonon dispersion relations at room temperature (○) and 750 K (+): (*a*) along the $(0\bar{1}4)$ direction; (*b*) along the (012) direction. The solid lines represent the transverse sound velocities. The dotted lines through the data points are intended only for a guide. The vertical dashed lines indicate the zone boundary.

interpretation of the diffuse scattering is then reminiscent of that found in some perovskites such as $BaTiO_3$ (Harada & Honjo, 1967). This would indicate an intimate relation between the LN and the perovskite structure. It must be emphasized, however, that this phenomenon is neither related to the ferroelectric–paraelectric phase transition in LN, nor does it show any appreciable critical behaviour (at least in the investigated temperature range). It would reflect an inherent instability of the structure, possibly a displacement of the $NbO_6$ chains against the Li's. It is not surprising then that the static disorder picture due to the defects in non-stoichiometric material as described has exactly the same behaviour. The semi-quantitative results and interpretations have to be supplemented by structure-factor calculations for the different disorder models. Direct Monte Carlo simulations of the defect structure and the related diffuse scattering are in progress.

We thank Professor E. Born (TU München) for supplying single crystals, as well as for fruitful discussions. The Alexander-von-Humboldt Fellowship for N. Zotov is gratefully appreciated. The work was also supported by funds of the BMFT under grant 03-SC3LMU.

### References

ABRAHAMS, S. C. & MARSH, P. (1986). *Acta Cryst.* B**42**, 61–68.
ABRAHAMS, S. C., HAMILTON, W. C. & REDDY, J. M. (1966). *J. Phys. Chem. Solids*, **27**, 1013–1018.
ABRAHAMS, S. C., LEVINSTEIN, H. J. & REDDY, J. M. (1966). *J. Phys. Chem. Solids*, **27**, 1019–1026.
ABRAHAMS, S. C., REDDY, J. M. & BERNSTEIN, J. L. (1966). *J. Phys. Chem. Solids*, **27**, 997–1012.
ADLHART, W. & HUBER, H. (1982). *J. Appl. Cryst.* **15**, 241–244.
ADLHART, W., TZAFARAS, N., SUENO, S., JAGODZINSKI, H. & HUBER, H. (1982). *J. Appl. Cryst.* **15**, 236–240.
BOLLMANN, W. & GERNAND, M. (1972). *Phys. Status Solidi (a)*, **9**, 301–308.
BOYSEN, H. & ADLHART, W. (1987). *J. Appl. Cryst.* **20**, 200–209.
BOYSEN, H. & ALTORFER, F. (1994). *Acta Cryst.* B**50**, 405–414.
CHOWDHURY, M. D., PECKHAM, G. E. & SAUNDERSON, D. H. (1978). *J. Phys. C*, **11**, 1671–1683.
DONNERBERG, H., TOMLINSON, S. M., CATLOW, C. R. A. & SCHIRMER, O. F. (1989). *Phys. Rev. B*, **40**, 11900–11916.
HARADA, J. & HONJO, G. (1967). *J. Phys. Soc. Jpn*, **22**, 45–57.
HOHLWEIN, D., HOSER, A. & PRANDL, W. (1986). *J. Appl. Cryst.* **19**, 262–266.
IVANOV, S. A., KORNEEV, A. E., KOLONTSOVA, E. V. & VENEVTSEV, YU. N. (1978). *Kristallografiya*, **23**, 1071–1073.
IYI, N., KITAMURA, K., IZUMI, F., YAMAMOTO, J. K., HAYASHI, T., ASANO, H. & KIMURA, S. (1992). *J. Solid State Chem.* **101**, 340–352.
LERNER, P., LEGRAS, C. & DUMAS, J. P. (1968). *J. Cryst. Growth*, **3**, 231.
LORENZ, G., NEDER, R., MARXREITER, J., FREY, F. & SCHNEIDER, J. (1993). *J. Appl. Cryst.* **26**, 632–635.
MEGAW, H. D. (1968). *Acta Cryst.* A**24**, 583–588.
MEGAW, H. D. & DARLINGTON, C. N. W. (1975). *Acta Cryst.* A**31**, 161–173.
METZGER, TH. (1993). Diploma Thesis, Technische Univ. München, Germany.
NASSAU, K. & LINES, M. E. (1970). *J. Appl. Phys.* **41**, 533–537.
NIIZEKI, N., YAMADA, T. & TOYODA, H. (1967). *Jpn. J. Appl. Phys.* **6**, 318.
PETERSON, G. E. & CARNEVALE, A. (1972). *J. Chem. Phys.* **56**, 4848–4851.
PROFFEN, T. & HRADIL, K. (1993). Proc. of the 31 Jahrestagung der DGK, 10–12 März 1993, Bochum, Germany. *Z. Kristallogr.* S**7**, 155.
RÄUBER, A. (1978). In *Current Topics in Material Science*, edited by E. KALDIS, Vol. 1, pp. 481–601. Amsterdam: North-Holland.
SCHIRMER, O. F., THIEMANN, O. & WÖHLECKE, M. (1991). *J. Phys. Chem. Solids*, **52**, 185–200.
SEARS, V. F. (1992). *Neutron News*, **3**, 26–37.
SMITH, R. T. & WELSH, F. S. (1971). *J. Appl. Phys.* **42**, 2219.
WEBER, V. K. (1967). *Acta Cryst.* **23**, 720.
WILLIS, B. T. M. & PRYOR, A. W. (1975). *Thermal Vibrations in Crystallography*. Cambridge Univ. Press.
WOOSTER, W. A. (1962). *Diffuse X-ray Reflexions from Crystals*. Oxford: Clarendon Press.
ZHDANOV, G. S., IVANOV, S. A., KOLONTSOVA, E. V. & KORNEEV, A. E. (1978). *Ferroelectrics*, **21**, 463–465.
ZOTOV, N. S., BOYSEN, H., FREY, F., METZGER, T. & BORN, E. (1994). *J. Phys. Chem. Solids*, **55**, 145–152.
ZOTOV, N. S., BOYSEN, H., SCHNEIDER, J. & FREY, F. (1994). Proc. of the III European Powder Diffraction Conference EPDIC3, 25–28 September 1993, Vienna, Austria, *Mat. Sci. Forum*, **166–169**, 631–636.